Measuring parameters of active galactic nuclei central engines with very high energy γ-ray flares

A. Neronov,[1,2]$\star$ D. Semikoz[3,4] and S. Sibiryakov[4,5]

[1]*INTEGRAL Science Data Center, Chemin d'Écogia 16, 1290 Versoix, Switzerland*
[2]*Geneva Observatory, 51 ch. des Maillettes, CH-1290 Sauverny, Switzerland*
[3]*APC, 10, rue Alice Domon et Leonie Duquet, 75205 Paris, France*
[4]*Institute for Nuclear Research of the Russian Academy of Sciences, 60th October Anniversary prospect 7a, Moscow 117312, Russia*
[5]*Theory Group, Department of Physics, CERN, CH-1211 Geneva 23, Switzerland*

ABSTRACT

We discuss a 'compact source' model of very high energy emission from blazars in which the variability time is determined by the blazar central engine. In this model, electron or proton acceleration close to the supermassive black hole is followed by the development of electromagnetic cascade in a radiatively inefficient accretion flow. Assuming such a model for the TeV blazar PKS 2155−304, we show that the variability properties of the TeV γ-ray signal observed during a bright flare from this source, such as the minimal variability time-scale and the recurrence period of the subflares, constrain the mass and the angular momentum of the supermassive black hole.

Key words: black hole physics – radiation mechanisms: non-thermal – BL Lacertae objects: individual: PKS 2155−304 – galaxies: nuclei – gamma-rays: theory.

1 INTRODUCTION

Recent observation of fast variability of TeV γ-ray emission from several TeV blazars (Aharonian et al. 2007; Albert et al. 2007) challenges the conventional model in which the TeV γ-rays are supposed to be produced at large distances from the blazar central engine, the supermassive black hole (BH). Within this conventional model, the γ-ray emitting blobs are assumed to travel to the parsec-scale distances along the active galactic nuclei (AGN) jet before emitting in the TeV energy band; it is believed that otherwise the γ-ray emission would be strongly absorbed in the accretion flow (see e.g. Ghisellini & Madau 1996). Since the radiative cooling time of the TeV emitting electrons is typically shorter than the time of propagation from the central engine to the TeV emission region, it is usually assumed that the TeV emitting particles are produced via shock acceleration locally in the emission region, rather than in the AGN central engine.

At the same time, the observed short variability time-scales $t_{\mathrm{var}} \sim$ a few minutes indicate that the TeV emission comes from very compact regions having the size in the comoving frame $\Delta x' \lesssim \delta(1+z)^{-1}ct_{\mathrm{var}}$, where δ is the bulk Doppler factor and z is the source redshift. This implies that in the static frame the longitudinal size

of the TeV emitting region is

$$\Delta x = \frac{\Delta x'}{\Gamma} \lesssim (1+z)^{-1}ct_{\mathrm{var}} \simeq 6 \times 10^{12}(1+z)^{-1}\left(\frac{t_{\mathrm{var}}}{200\,\mathrm{s}}\right)\,\mathrm{cm}\,, \tag{1}$$

where we assume that the bulk Lorentz factor $\Gamma \sim \delta$. This is comparable to the minimal possible scale set up by the gravitational radius of the central supermassive BH:

$$R_{\mathrm{g}} = GM_{\mathrm{BH}}/c^2 \simeq 1.5 \times 10^{12}\left(M_{\mathrm{BH}}/10^7\,\mathrm{M_\odot}\right)\,\mathrm{cm}\,. \tag{2}$$

Even if one assumes that the TeV emitting plasma blobs are produced close to the BH, which would explain their initially small size, it is not clear how the blobs propagating downstream the relativistic jet can retain this size up to large distances, unless they have unreasonably large bulk Lorentz factors. This problem has recently led to a suggestion (Begelman, Fabian & Rees 2008) that the TeV flares may not be triggered by the BH but rather are results of enhanced emission intrinsic to the jet.

However, even in that case, to explain the observed rapid variability, the TeV γ-ray emitting blobs have to travel with quite large bulk Lorentz factors, $\Gamma \gg 1$. Such Lorentz factors are in contradiction with the radio observations of the motion of hotspots in the parsec-scale jets. Moderate apparent speeds of the blobs of the parsec-scale jets, revealed by radio observations, combined with an estimate of the number of parent objects of TeV blazars, would give much smaller values of the bulk Lorentz factors, $\Gamma \sim 1$ (Henri & Saugé 2006). For example, to explain the fast variability of the 2006 July TeV flare of PKS 2155−304 (Aharonian et al. 2007) the

$\star$E-mail: andrii.neronov@obs.unige.ch

bulk Lorentz factor required by the mechanism of TeV emission in the parsec-scale jet should be $\Gamma > 50$ (Aharonian et al. 2007; Begelman et al. 2008). At the same time, the direct observations of the apparent velocity of hotspots in PKS 2155−304 jet at the projected distance (1/2) parsecs give the value $v_{app} = (0.9 \pm 0.3)c$ (Piner, Pant & Edwards 2008). Assuming that the viewing angle is not too small, $\theta \gtrsim 1°$, this yields $\Gamma \lesssim 10$ at the distance of a few tens of parsecs from the central engine.

Both the problems of the fast variability and the small observed Lorentz factors at parsec distances could be naturally resolved if the site of the very high energy (VHE) γ-ray production is located closer to the AGN central engine, at significantly subparsec distances. If the VHE emitting region is moving relativistically towards the observer with a bulk Lorenz factor Γ, the variability time-scale limits the distance R of the γ-ray production site from the central engine (see e.g. Celotti, Fabian & Rees 1998):

$$R \sim \Delta x \, \Gamma^2 \leq 1.5 \times 10^{16}(1+z)^{-1} \left(\frac{t_{var}}{200\,s} \right) \left(\frac{\Gamma}{50} \right)^2 cm. \qquad (3)$$

An immediate difficulty is, however, that at such distances the accretion flow on to the BH can be opaque to the γ-rays (see e.g. Blandford & Levinson 1995).

The problem of opacity of the compact source does not arise in the case of low-luminosity AGN that accrete at significantly sub-Eddington rates (Celotti et al. 1998). In these sources, the accretion flow is described within the framework of the radiatively inefficient accretion flow (RIAF) models (Rees et al. 1982; Narayan & Yi 1994, 1995; Narayan 2002) in which most of the gravitational energy extracted from the accreted matter is converted into internal energy, rather than into radiation. The possibility of escape of the VHE γ-rays from the vicinity of the AGN central engine is best illustrated by the nearby low-luminosity radio galaxy M87, which was recently found to be a source of the variable TeV γ-ray emission (Aharonian et al. 2003, 2006; Albert et al. 2008), most probably coming from a compact source (Neronov & Aharonian 2007; Rieger & Aharonian 2008b).

In the compact source model, the VHE γ-ray emission is triggered by high-energy particles accelerated close to the BH via one of the possible mechanisms (see e.g. Lovelace 1976; Lesch & Pohl 1992; Kardashev 1995; Bednarek & Protheroe 1999; Neronov et al. 2002; Neronov & Semikoz 2002; Neronov, Tinyakov & Tkachev 2005; Rieger & Aharonian 2008a; Neronov, Semikoz & Tkachev 2008). In this case, the spectral and timing characteristics of the VHE emission are directly linked to the physics of the processes taking place close to the supermassive BH, which naturally explains the variability of the signal on the shortest possible time-scale.

Within the AGN unification scheme, the TeV blazars (high-energy peaked BL Lacs) are assumed to be the beamed versions of the low-luminosity radio galaxies similar to M87 (Browne 1983; Giroletti et al. 2004, 2006). Since the only difference between the TeV blazars and the low-luminosity radio galaxies is their orientation with respect to the line of sight, the compact source model can be applicable also in the case of TeV blazars.

In what follows, we adopt this point of view and develop a compact source model of high-energy activity of TeV blazars. We demonstrate that within such compact source model, the characteristics of the fast variable VHE emission can be used to constrain the parameters of the AGN central engine, in particular, the density and luminosity of the accretion flow, the BH mass and spin. We illustrate this possibility on the particular example of the bright PKS 2155−304 flare detected by the HESS telescope in 2006 July

(Aharonian et al. 2007). This flare consists of a number of well-pronounced subflares which exhibit quasi-periodic recurrence. We show that the rise time and the recurrence period of the subflares can be directly related to the light-crossing time and the period of rotation over the last stable orbit around a $M_{BH} \sim 10^7\,M_\odot$ BH.[1]

The paper is organized as follows. In Section 2, we discuss the qualitative features of the model, including particle acceleration and propagation through the RIAF environment. The possibility of a new interpretation of the observational data within such a model is demonstrated in Section 3, where we find the constraints on the BH mass and angular momentum imposed by the timing analysis of the bright TeV flare of PKS 2155−304. We summarize our results in Section 4.

2 COMPACT SOURCE MODEL OF THE TeV BLAZARS

In the compact source model, the VHE γ-ray emission region is assumed to be situated in the vicinity of the AGN central engine, rather than at parsec-scale distances. This fact implies two main differences of this model from a generic 'relativistically moving blob' model of VHE emission from blazars. First, the high-energy particles responsible for the VHE emission can be injected into the γ-ray emission region by the AGN central engine, rather than only by a process (shock acceleration) intrinsic to the blob. Secondly, the characteristics of the γ-ray emission are determined not only by the intrinsic properties of the blob, but also by the effects of propagation of the high-energy particles through the matter and radiation environment created by the accretion flow. However, as we discuss below, the compact source model to some extent includes the blob model: the electromagnetic cascade, which develops as a result of the propagation of high-energy particles through the accretion flow environment, leads to the formation of a relativistically moving blob of secondary cascade particles. In the following sections, we consider general features of particle acceleration and propagation in the compact source model of TeV blazars.

2.1 Particle acceleration and 'direct' γ-ray emission from the acceleration region

A number of mechanisms of particle acceleration in the vicinity of the central BH have been proposed in the literature (see e.g. Lovelace 1976; Lesch & Pohl 1992; Kardashev 1995; Bednarek & Protheroe 1999; Neronov et al. 2002; Neronov & Semikoz 2002; Neronov et al. 2005; Rieger & Aharonian 2008a; Neronov et al. 2008). In this section, we summarize some common features of the acceleration models which are related to the fact that the acceleration proceeds in a compact region of the size comparable to the BH horizon and are independent of the details of the acceleration mechanism.

A conventional dimensional estimate of maximal possible energies of particles of charge e accelerated in a region of the size $R \sim R_g$ with the magnetic field B is

$$E_{max} = \kappa e B R_g \simeq 10^{19} \kappa \left(\frac{B}{10^4\,G} \right) \left(\frac{M_{BH}}{10^7\,M_\odot} \right) eV, \qquad (4)$$

where $\kappa \leq 1$ is the efficiency of a particular acceleration mechanism. This maximal energy is, however, not always achieved because of

---

[1] This mass estimate is different from the value $\sim 10^9\,M_\odot$ quoted by Aharonian et al. (2007). We will comment on this discrepancy in Section 3.3.

the strong energy losses experienced by the accelerated particles. The 'minimal' energy loss channel is the loss on the curvature radiation (Levinson 2000; Aharonian & Neronov 2005; Neronov et al. 2008), which limits the particle energies to

$$\frac{E_{cur}}{mc^2} \leq \left(\frac{3R_g^2 \kappa B}{2e}\right)^{1/4} \simeq 3 \times 10^9 \kappa^{1/4} \left(\frac{M_{BH}}{10^7\,M_\odot}\right)^{1/2} \left(\frac{B}{10^4\,G}\right)^{1/4},$$

$$(5)$$

where m is the particle mass. Here, we normalize the magnetic field to the value 10^4 G typical for the central engine of an AGN with a $10^7\,M_\odot$ BH. Additional energy losses, caused by the interactions of the accelerated particles with the matter and radiation backgrounds produced by the accretion flow (see Section 2.2 below), lead to further reduction of the maximal attainable energy. If the magnetic field in the acceleration region is not ordered, the energies of the accelerated particles are reduced because of the strong synchrotron energy loss.

Radiative energy losses which accompany particle acceleration [curvature, synchrotron, inverse-Compton (IC)] result in the γ-ray emission directly from the acceleration region. If the resulting γ-rays are not completely absorbed during their propagation through the photon background created by the accretion flow, this 'direct' γ-ray emission can, in principle, provide an observable signature of the compact source model. We will return to this point in Section 2.4.

Since the maximal energies of particles are determined by the balance of the acceleration and energy-loss rates, all the work done by the electric field is dissipated via the available energy-loss channels. For each charged particle, the energy-loss rate is about the acceleration rate, $dE/dt \sim e\kappa Bc$, where we assume that the accelerating electric field strength is $\sim \kappa B$. The maximal possible density of particles in the acceleration region, $n_q \sim \kappa B/eR$, is determined by the condition that a charge redistribution cannot screen the electric field. One estimates the total power extracted from the acceleration region by multiplying the energy-loss rate of each particle on the maximal possible particle density and the volume of the acceleration region, $V \sim R_g^3$; this yields

$$P_{tot} \simeq n_q R_g^3 (dE/dt)$$

$$\simeq 5 \times 10^{42} \kappa^2 \left(\frac{M_{BH}}{10^7\,M_\odot}\right)^2 \left(\frac{B}{10^4\,G}\right)^2 \text{erg s}^{-1}.$$

$$(6)$$

Comparing this estimate to the apparent luminosity of a bright TeV flare (found under the assumption that the radiation is isotropic), $L_{iso} \simeq 10^{46}$ erg s^{-1}, one concludes that the energetics of such a flare is compatible with the compact source model if the TeV emission is beamed into the solid angle $\Omega/4\pi \lesssim 10^{-3}$. The emission from the compact source is expected to be anisotropic, with the direction of the beam of high-energy particles and/or photons set up by the direction of the magnetic field.

A fraction of the work done by the accelerating electric field is carried away by the flux of accelerated particles (a relativistic wind). In the case of electrons, this fraction is usually negligible. In the case of protons or heavy nuclei, the power of the relativistic particle wind, P_p, can be estimated as

$$P_p \sim n_q R_g^2 c \min\{E_{cur}, E_{max}\}$$

$$\simeq \begin{cases} 10^{42} \kappa^{5/4} \left(\dfrac{M_{BH}}{10^7\,M_\odot}\right)^{3/2} \left(\dfrac{B}{10^4\,G}\right)^{5/4} \dfrac{\text{erg}}{\text{s}}, & E_{cur} < E_{max} \\[2ex] 5 \times 10^{42} \kappa^2 \left(\dfrac{M_{BH}}{10^7\,M_\odot}\right)^2 \left(\dfrac{B}{10^4\,G}\right)^2 \dfrac{\text{erg}}{\text{s}}, & E_{cur} > E_{max} \end{cases}$$

$$(7)$$

This order-of-magnitude estimate does not take into account a possible special geometry of the accelerating field. If, for instance, particles are accelerated in parallel magnetic and electric fields in the polar cap regions of BH magnetospheres, the curvature radii of particle trajectories can be somewhat larger than R_g and, respectively, the maximal attainable energies and the power of the particle beam can be higher (Neronov et al. 2008).

The high-energy particles and radiation emitted from the acceleration region are injected into the accretion flow. The form of the γ-ray signal produced by the interaction of the accelerated particles with the radiation coming from the accretion flow depends sensitively on the geometry of the central engine. The precise determination of this signal should involve detailed numerical modelling which is beyond the scope of this paper. Below we limit ourselves to the order-of-magnitude estimates which highlight the qualitative features of the problem.

2.2 Radiatively inefficient accretion flow

In this section, we summarize the general properties of the radiation produced by the accretion flow. As it is mentioned in the Introduction, the TeV blazars belong to the class of low-luminosity radio galaxies in which the accretion is conventionally described in the framework of RIAF models (see e.g. Narayan 2002, and references therein) relevant for sources in which the accretion rate $\dot{M}$ is small in the Eddington units:

$$\dot{M} \ll \dot{M}_{Edd} \equiv \frac{L_{Edd}}{0.1c^2} \simeq 0.2 \left(\frac{M_{BH}}{10^7\,M_\odot}\right) M_\odot\,\text{yr}^{-1},$$

$$(8)$$

where $\dot{M}_{Edd}$ is the Eddington accretion rate.

The low radiative efficiency of the accretion flow is attributed to the low matter density which leads to inefficient cooling of electrons and ions in the accretion flow. As a result, a large fraction of the released gravitational energy, instead of being dissipated in the form of radiation, is stored in the internal energy of matter. This energy either disappears under the horizon or is ejected in an outflow.

Large internal energy of matter does not allow formation of a geometrically thin, optically thick accretion disc. Instead, the accreting matter forms around the BH a hot optically thin gaseous torus (Rees et al. 1982). In RIAF models, the accretion torus typically consists of two-temperature plasma with both electrons and ions being mildly relativistic. The radiation of the plasma is entirely produced by electrons via three main mechanisms: synchrotron radiation, comptonization of the latter and bremsstrahlung.

The synchrotron radiation contributes to the far-infrared part of the spectrum. The characteristic synchrotron emission energy is

$$\epsilon_{synch} = \frac{\hbar e B}{m_{ec}} \langle \gamma_e^2 \rangle \simeq 5 \times 10^{-3} \left(\frac{B}{10^4\,G}\right) \left(\frac{T_e}{1\,MeV}\right)^2 \text{eV},$$

$$(9)$$

where B is the magnetic field in the inner part of the accretion torus, m_e is the electron mass, $\langle \gamma_e^2 \rangle$ is the mean-square γ-factor of electrons, T_e is the electron temperature and we have used that for mildly relativistic electrons

$$\langle \gamma_e^2 \rangle \sim 10 \left(\frac{T_e}{m_ec^2}\right)^2.$$

$$(10)$$

One of the parameters of the RIAF models is the ratio β of the gas pressure $p_{gas} = nm_p v_{th}^2/3$ to the magnetic pressure $p_{magn} = B^2/4\pi$. Here, n is the gas density, m_p is the proton mass and v_{th} is the thermal velocity of protons which can be estimated as the Keplerian velocity at the corresponding distance, $v_{th}(R) \approx (R_g/R)^{1/2}$. With the use of

parameter β, the magnetic field is estimated as

$$B(R) = \left[\frac{4\pi}{3}\beta^{-1}n(R)m_{\mathrm{p}}v_{\mathrm{th}}^2(R)\right]^{1/2}$$
$$\simeq 10^4\beta^{-1/2}\left(\frac{R_{\mathrm{g}}}{R}\right)^{1/2}\left[\frac{n(R)}{10^{10}\,\mathrm{cm}^{-3}}\right]^{1/2}\,\mathrm{G}\,. \tag{11}$$

Note that we normalize the matter density in the BH vicinity to the value $10^{10}\,\mathrm{cm}^{-3}$, typical for the case of a $10^7\,\mathrm{M}_\odot$ BH in the RIAF models, cf. Narayan & Yi (1995).

If the matter density changes with the distance as $n(R) \sim R^{-\gamma}$ (in the RIAF models $1/2 \le \gamma \le 3/2$, Lu, Li & Gu 2004), the magnetic field decreases as $B \sim R^{-(\gamma+1)/2}$, so that the synchrotron cooling time

$$t_{\mathrm{synch}} = \frac{6\pi m_{\mathrm{ec}}^2}{\sigma_{\mathrm{T}}B^2\gamma_{\mathrm{e}}} \simeq 1.3\left(\frac{B}{10^4\,\mathrm{G}}\right)^{-2}\left(\frac{T_{\mathrm{e}}}{1\,\mathrm{MeV}}\right)^{-1}\,\mathrm{s} \tag{12}$$

increases with the distance as $t_{\mathrm{synch}} \sim R^{(\gamma+1)}$. Here, $\sigma_{\mathrm{T}} = 0.665 \times 10^{-24}\,\mathrm{cm}^2$ is the Thomson cross-section. The synchrotron cooling is efficient only close to the BH horizon. Indeed, the synchrotron cooling time grows with R faster than the dynamical time-scale given by the free-fall time:

$$t_{\mathrm{ff}} \simeq \sqrt{R^3/GM_{\mathrm{BH}}}. \tag{13}$$

Thus, the bulk of the synchrotron emission is produced in the vicinity of the horizon. Numerical simulations (Narayan 2002) confirm this qualitative result.

The synchrotron emission in the RIAF models is damped due to self-absorption. The self-absorption coefficient has the form (Pacholczyk 1970)

$$\alpha_{\mathrm{SA}}(\epsilon) = \frac{\pi\hbar e^2 m^2 c^5 n}{2\sqrt{3}T_{\mathrm{e}}^3\epsilon}I(x), \tag{14}$$

where

$$x = \frac{2m^3c^5\epsilon}{3\hbar eBT_{\mathrm{e}}^2} \tag{15}$$

and the function $I(x)$ is given explicitly in the Appendix A. Equating $\alpha_{\mathrm{SA}}^{-1}$ to the size of the synchrotron emission region, which we take to be of the order of the gravitational radius, one finds the photon energy at which the synchrotron emission becomes optically thin

$$\epsilon_{\mathrm{SA}} \simeq 37\,\epsilon_{\mathrm{synch}}. \tag{16}$$

As discussed in the Appendix A, the numerical coefficient in this formula mildly depends on the parameters of the accretion flow. We omit this dependence in what follows.

Since $\epsilon_{\mathrm{SA}} > \epsilon_{\mathrm{synch}}$, the maximum of the synchrotron power is emitted at the energy ϵ_{SA}. To estimate the synchrotron luminosity we approximate the spectrum by thermal radiation up to ϵ_{SA}. This yields

$$L_{\mathrm{synch}} = 4\pi R_{\mathrm{synch}}^2\frac{2T_{\mathrm{e}}}{c^2}\int_0^{\epsilon_{\mathrm{SA}}}\frac{\epsilon^2 d\epsilon}{(2\pi\hbar)^3}\,, \tag{17}$$

where R_{synch} is the size of the synchrotron emission region. Substituting $R_{\mathrm{synch}} \approx R_{\mathrm{g}}$, we obtain

$$L_{\mathrm{synch}} \simeq 3.2 \times 10^{39}\left(\frac{M_{\mathrm{BH}}}{10^7\,\mathrm{M}_\odot}\right)^2\left(\frac{B}{10^4\,\mathrm{G}}\right)^3\left(\frac{T_{\mathrm{e}}}{1\,\mathrm{MeV}}\right)^7\,\mathrm{erg\,s}^{-1}\,. \tag{18}$$

The part of the synchrotron spectrum above ϵ_{SA} gives small contribution to the total synchrotron power because of the exponential cut-off in the synchrotron emission function. An immediate consequence of this cut-off is that the bulk of the synchrotron photons has energies $\epsilon \lesssim \epsilon_{\mathrm{SA}} \simeq 0.2\,\mathrm{eV}$.

The synchrotron radiation is upscattered by IC process into the optical band:

$$\epsilon_{\mathrm{IC}} \sim \epsilon_{\mathrm{SA}}\langle\gamma_{\mathrm{e}}^2\rangle \simeq 4\left(\frac{B}{10^4\,\mathrm{G}}\right)\left(\frac{T_{\mathrm{e}}}{1\,\mathrm{MeV}}\right)^4\,\mathrm{eV}\,. \tag{19}$$

To estimate the luminosity of the accretion flow in this range, we note that the IC volume emissivity at distance R from the BH is (Rybicki & Lightman 2004)

$$\frac{dL_{\mathrm{IC}}}{dV} = \frac{4}{3}\sigma_{\mathrm{T}}cn(R)\langle\gamma_{\mathrm{e}}^2(R)\rangle U_{\mathrm{synch}}(R), \tag{20}$$

where $\langle\gamma_{\mathrm{e}}^2(R)\rangle$ is the mean-square γ-factor of electrons at this distance and $U_{\mathrm{synch}}(R) \simeq L_{\mathrm{synch}}/(4\pi R^2 c)$ is the energy density of the synchrotron radiation. Integrating over the volume, we obtain

$$L_{\mathrm{IC}} \simeq \frac{4}{3}L_{\mathrm{synch}}\sigma_{\mathrm{T}}\int n_{\mathrm{e}}(R)\langle\gamma_{\mathrm{e}}^2(R)\rangle dR\,. \tag{21}$$

Depending on the radial profiles of the electron density and temperature, the integral in equation (21) is saturated either close to the BH horizon [for the radial profiles steeper than $n(R)\langle\gamma_{\mathrm{e}}^2(R)\rangle \sim R^{-1}$] or in a region which is much larger than the size of the BH. In the numerical simulations of RIAF models, one finds the typical size R_{IC} of the IC emission region to be of the order of $100R_{\mathrm{g}}$ (Narayan 2002). As a crude estimate, let us consider the case when the integral in equation (21) is saturated at the upper limit. Then,

$$L_{\mathrm{IC}} \simeq 0.4 \times 10^{39}\left(\frac{L_{\mathrm{synch}}}{10^{39}\,\mathrm{erg\,s}^{-1}}\right)\left(\frac{R_{\mathrm{IC}}}{10^{14}\,\mathrm{cm}}\right)$$
$$\times\left[\frac{n(R_{\mathrm{IC}})}{10^8\,\mathrm{cm}^{-3}}\right]\left[\frac{T_{\mathrm{e}}(R_{\mathrm{IC}})}{1\,\mathrm{MeV}}\right]^2\,\mathrm{erg\,s}^{-1}\,. \tag{22}$$

Note that in the above estimate, we took into account that the electron density and temperature at the distance R_{IC} are lower than near the BH.

Finally, we consider the bremsstrahlung radiation. It contributes primarily into the X-ray/soft γ-ray band with the total power typically comparable or lower than that of the synchrotron radiation. The bremsstrahlung emission power is proportional to n^2, so that the bremsstrahlung luminosity from a region of the size R is $P_{\mathrm{brems}} \sim n(R)^2R^3$. If the radial density falls down slower than $n(R) \sim R^{-3/2}$ (as it is the case in typical RIAF models), the bulk of the bremsstrahlung flux is produced at large distances. Numerical modelling of the radiatively inefficient accretion shows that the bremsstrahlung is produced mainly at large distances from the BH, $R_{\mathrm{brems}} \sim 10^5 \times R_{\mathrm{g}}$ (Narayan 2002).

To summarize, the properties of RIAF important for the high-energy particle propagation are as follows. Matter distribution in a typical RIAF is characterized by a rather shallow radial density profile $[n(R) \sim R^{-1/2}]/R^{-3/2}$, so that the central matter density is rather low. At the same time, due to the large non-dissipated mechanical energy of the accreting matter the magnetic field produced by the RIAF can be strong close to the central BH (equation 11). The radiation environment created by a RIAF has an 'onion-like' structure with the infrared synchrotron emission produced close to the BH, infrared/optical IC emission produced in a larger region of the size $\sim 100R_{\mathrm{g}}$ and X-ray/soft γ-ray bremsstrahlung emission produced in a region of the size $\sim 10^5R_{\mathrm{g}}$.

To conclude this section, let us make the following comment. The estimates presented above strongly depend on the values of the parameters of the accretion flow such as electron temperature, density and magnetic field. These characteristics vary significantly in different RIAF models. The estimates presented in this section should be considered as indicative. A more detailed analysis of the
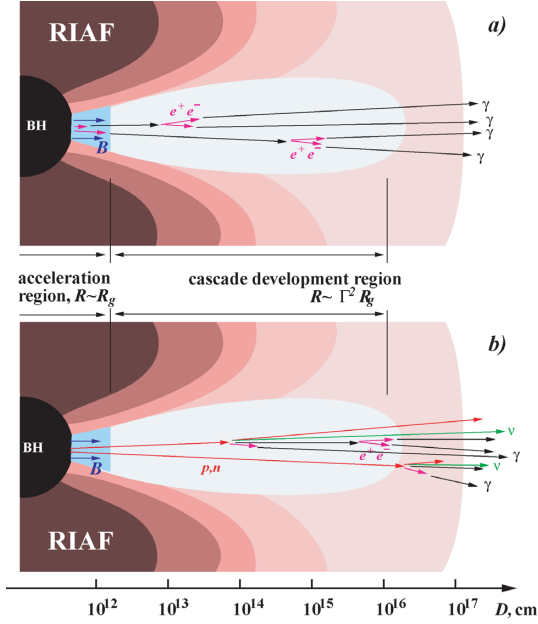
Figure 1. Schematic representation of the two possible scenarios for the γ-ray emission from the compact source. Particles (electrons in the upper panel, protons in the lower panel) are initially accelerated in a compact region of the size of about R_g, shown as a blue-shaded region. Particles which escape from the acceleration region initiate a cascade in the RIAF, at the distances $R \gg R_g$, shown as a light-blue shaded region.

radiative background can be done using numerical simulations in each particular RIAF model.

2.3 Propagation of the high-energy particles through the accretion flow background

The compact particle accelerator close to the BH produces emission with the total power P_{tot}, equation (6). As discussed above, the partition of this energy between the γ-ray component and the accelerated matter depends on the type of accelerated particles (see Fig. 1). If the accelerated particles are electrons, the power goes completely into γ-rays, while in the case of the proton acceleration a significant part of P_{tot} can remain in the high-energy particle beam, see equation (7). The primary γ-rays and protons propagate through and interact with the matter and radiation background created by RIAF. Interactions of high-energy particles give rise to electromagnetic cascades that redistribute the power initially contained in the highest energy particles to lower energy bands.

Since the rates of interactions of electrons and γ-rays are significantly different from those of protons, we consider these two cases separately.

2.3.1 Electrons and γ-rays

The highest energy γ-rays produce pairs in interactions with the soft photon background inside the compact source. The cross-section of photon–photon pair-production depends on the center-of-mass energy of colliding photons:

$$s = E\epsilon(1 - \cos\theta)/2m_e^2 , \qquad (23)$$

where E and ϵ are the energies of the photons and θ is the collision angle. Starting from the threshold at $s = 1$, the cross-section rapidly increases achieving the maximum $\sigma_{\gamma\gamma} \approx 1.3 \times 10^{-25}$ cm^2

at $s \approx 4$, and then decreases as $s^{-1} \ln s$. Because of relatively narrow distribution of $\sigma_{\gamma\gamma}(s)$, γ-rays interact most efficiently with the optical/infrared background photons of energy $\epsilon \simeq 1(E_\gamma/1\,\text{TeV})^{-1}$ eV. This interaction leads to absorption of the γ-rays. In order for the VHE emission to escape from the vicinity of the BH, the optical depth of this process should be less than 1. Let us consider, the contributions of the various backgrounds produced by RIAF to the optical depth, case by case.

We start with the synchrotron background. This background is produced in the vicinity of the BH, $R_{synch} \approx R_g$. Consequently, its interaction with the VHE emission strongly depends on the geometry of the inner part of the accretion disc and acceleration region. The situation is still more complicated because of the exponential dependence of the density of the synchrotron background photons on energy (Pacholczyk 1970):

$$n_{synch}(\epsilon) = n_{synch}(\epsilon_{SA})I(x)/I(x_{SA}) , \quad \epsilon > \epsilon_{SA} , \qquad (24)$$

where the function $I(x)$ is given in equation (A2) and x is defined in equation (15). The density $n_{synch}(\epsilon_{SA})$ at the maximum of the synchrotron spectrum can be estimated as

$$n_{synch}(\epsilon_{SA}) = \frac{L_{synch}}{4\pi R_{synch}^2 \epsilon_{SA} c}$$
$$\simeq 10^{17} \left(\frac{L_{synch}}{10^{40}\,\text{erg s}^{-1}}\right) \left(\frac{R_{synch}}{10^{12}\,\text{cm}}\right)^{-2} \left(\frac{\epsilon_{SA}}{0.2\,\text{eV}}\right)^{-1}\text{cm}^{-3} . \qquad (25)$$

Using equation (24), one finds that because of the sharp cut-off in the synchrotron spectrum above the energy $\epsilon_{SA} \sim 0.2$ eV, γ-rays with energy $E_\gamma \sim 1$ TeV escape through the synchrotron background, $\tau_{\gamma\gamma}(E_\gamma = 1\,\text{TeV}) \sim 1$, if $R_{synch} \sim 10^{12}$ cm and $L_{synch} \lesssim 10^{40}$ erg s^{-1}. On the other hand, our crude estimates indicate that the spectrum of the escaping γ-rays should be sharply cut-off at the energy $E_\gamma \simeq 5(\epsilon_{SA}/0.2\,\text{eV})^{-1}$ TeV, since $\tau_{\gamma\gamma}$ rapidly grows to $\tau_{\gamma\gamma} \gg 1$ at this energy. One should note, however, that the details of the behaviour of the spectrum close to the cut-off strongly depend on the details of the spatial distribution of the synchrotron emission. Since the threshold of the pair production, $s = 1$ (see equation 23), depends on the angle θ between the γ-ray and synchrotron photon velocities, the anisotropy of the synchrotron emission can result in a shift of the cut-off in the γ-ray spectrum towards higher energies.

VHE γ-rays produced outside of the synchrotron emission region, or those which escape from it, pass through the IC background with the photon density:

$$n_{IC} = \frac{L_{IC}}{4\pi R_{IC}^2 \epsilon c}$$
$$\simeq 1.7 \times 10^{11} \left(\frac{L_{IC}}{10^{39}\,\text{erg s}^{-1}}\right) \left(\frac{R_{IC}}{10^{14}\,\text{cm}}\right)^{-2} \left(\frac{\epsilon}{1\,\text{eV}}\right)^{-1}\text{cm}^{-3} . \qquad (26)$$

The optical depth of this background for the TeV γ-rays can be estimated as

$$\tau_{\gamma\gamma}^{IC}(E_\gamma) = \sigma_{\gamma\gamma} n_{IC} R_{IC}$$
$$\simeq 2.2 \left(\frac{L_{IC}}{10^{39}\,\text{erg s}^{-1}}\right) \left(\frac{R_{IC}}{10^{14}\,\text{cm}}\right)^{-1} \left(\frac{E_\gamma}{1\,\text{TeV}}\right) . \qquad (27)$$

Thus, the inner part of the accretion flow is transparent for the TeV γ-rays if

$$L_{IC} \lesssim 0.5 \times 10^{39} \left(\frac{R_{IC}}{10^{14}\,\text{cm}}\right) \left(\frac{E_\gamma}{1\,\text{TeV}}\right)^{-1} \text{erg s}^{-1} . \qquad (28)$$

Finally, the background of the bremsstrahlung radiation does not affect propagation of the high-energy γ-rays. This is due to two reasons: the low density of the corresponding photons and their relatively weak interaction with the VHE γ-rays because of the $1/s$ suppression of the photon–photon cross-section.

Thus, in the case when the luminosity of the accretion flow is as low as $L_{acc} \lesssim 10^{40}$ erg s^{-1}, the VHE γ-ray emission can originate directly from the vicinity of the BH. It can be, for example, the direct synchrotron/curvature emission which accompanies the acceleration process. This possibility is illustrated schematically in Fig. 1 (upper panel). Otherwise, if the synchrotron luminosity of RIAF is significantly above 10^{40} erg s^{-1} and/or the IC luminosity exceeds the limit (equation 28), the VHE γ-ray emission must be produced outside the corresponding radiation regions. This is possible if the primary accelerated particles are protons.

2.3.2 Protons

Protons with energies above the threshold

$$E_{th} = \frac{m_\pi(m_\pi + 2m_P)}{4\epsilon} \sim 8 \times 10^{16} \left(\frac{\epsilon}{1\,\text{eV}}\right)^{-1} \text{eV} \qquad (29)$$

loose energy in the interactions with the infrared photons of energy ϵ via pion production. Near the threshold, the cross-section is dominated by the single pion production resonance $\sigma_{p\gamma} \sim 6 \times 10^{-28}$ cm^2; in this regime, proton gives only 20 per cent of its energy to the pion. At higher proton energies, the photo-pion production cross-section decreases down to $\sigma_{p\gamma} \sim 10^{-28}$ cm^2, while the proton energy loss in every interaction increases up to 50 per cent. Thus, in both the cases, protons lose most of their energy at similar distance.

For high synchrotron background, $L_{synch} \sim 10^{42}$ erg s^{-1}, protons with energies $E_p > 10^{18}$ eV cannot escape from the acceleration region:

$$\tau_{p\gamma}^{synch}\left(E_p > 10^{18}\,\text{eV}\right) = \sigma_{p\gamma} n_{synch} R_{synch}$$
$$\sim 10^3 \left(\frac{L_{synch}}{10^{42}\,\text{erg s}^{-1}}\right)\left(\frac{R_{synch}}{10^{12}\,\text{cm}}\right)^{-1}$$
$$\times \left(\frac{\epsilon}{0.2\,\text{eV}}\right)^{-1}. \qquad (30)$$

On the other hand, protons with energy $E_p < 10^{18}$ eV interact only with exponential tail of the synchrotron emission and escape from this region.

During the propagation through the IC emission region at the distance scales $R \sim 100 R_g$, protons interact with the IC photon background, so that the optical depth is

$$\tau_{p\gamma}^{IC} = \sigma_{p\gamma} n_{IC} R_{IC}$$
$$\simeq 0.2 \left(\frac{L_{IC}}{10^{41}\,\text{erg s}^{-1}}\right)\left(\frac{R_{IC}}{10^{14}\,\text{cm}}\right)^{-1}\left(\frac{\epsilon}{1\,\text{eV}}\right)^{-1}. \qquad (31)$$

The power of the absorbed proton flux is converted into the products of pion decays: neutrinos, γ-rays and electrons of the energies $\sim 0.1 E_p$. Obviously, the neutrinos freely escape from the production region.

Naively, from the above discussion of propagation of γ-rays, one would expect that γ-rays are not able to escape from such a dense IC background. However, this is incorrect. The point is that the energies of the γ-rays produced in the neutral pion decays are much above the energy corresponding to the maximum of the pair production rate on the IC background. For example, for the 10^{17} eV γ-rays, the cross-section of the pair production on the IC background is $s/\ln s \sim 10^4$ times smaller than the peak value, so that it is of the order of $p\gamma$

interaction cross-section. Thus, the mean free path of the secondary γ-rays is comparable to the mean free path of the primary protons, and is of the order of the size of the IC radiation region. These γ-rays can give rise to electromagnetic cascades redistributing energy into TeV γ-rays. The drawback of this mechanism of TeV emission is its low efficiency (Neronov & Semikoz 2003) due to the fact that the TeV γ-rays which are observed at infinity can be produced only in the surface layer of the IC radiation region, where the optical depth for the TeV radiation drops to the values of the order of 1. On the other hand, this mechanism should result in strong multi-GeV emission which can escape through the whole IC radiation region without significant absorption. This implies that if this mechanism is indeed responsible for the TeV emission in (some of) the TeV blazars, it should lead to a strong signal in the multi-GeV band accessible for the Fermi (GLAST) satellite.[2]

Apart from the interactions with soft radiation background, protons can also interact with the matter in the jet. The optical depth of protons with respect to this process is estimated as

$$\tau_{pp} = \sigma_{pp} n_p(R) R , \qquad (32)$$

where $n_p(R)$ is the matter density in the jet at the distance R. Taking the pp interaction cross-section at energies $E_p \sim 10^{18}$ eV to be equal to $\sigma_{pp} \simeq 10^{-25}$ cm^2, we obtain

$$\tau_{pp} \simeq 0.1 \left[\frac{n_p(R)}{10^8\,\text{cm}}\right]\left(\frac{R}{10^{16}\,\text{cm}}\right). \qquad (33)$$

Particle multiplicity in pp collisions at $E_p \sim 10^{18}$ eV is about $N \sim 100$–200 (see e.g. Heiselberg 2001 for a review). Thus, every collision of a 10^{18} eV proton with a background proton produces ~ 100 photons with $E_\gamma = 5 \times 10^{15}$ eV from π^0, ~ 100 neutrinos with the same energy from $\pi^\pm$ decays and ~ 100 electrons and positrons. All neutrinos escape from the interaction region, while electrons, positrons and photons give rise to an electromagnetic cascade. As we discuss in the next section, this provides a link with the standard picture of VHE emission by relativistic blobs in the jet. The limitation of this mechanism is that it requires rather large densities of matter in the jet, see equation (33).

To summarize, the qualitative analysis of this section shows that production of VHE γ-rays can, in principle, be possible within the compact source model with proton acceleration, see Fig. 1, lower panel. Still, the details of the mechanism of conversion of the proton flux power into the power of TeV γ-ray emission are yet to be worked out.

2.4 Particle cascade in the accretion flow: a link to the 'relativistic blob in the jet' picture

The $\gamma\gamma$, $p\gamma$ and pp interactions taking place during the propagation of the high-energy particles through the RIAF environment give rise to electromagnetic cascades, which redistribute the power initially contained in the highest energy particles to the lower energy bands. This is expected to result in the broad-band (radio-to-γ-ray) electromagnetic emission from the cascade.

To large extent, this emission can be described by the conventional synchrotron – self-Compton and/or synchrotron – external Compton models based on the picture of relativistically moving blobs of plasma in the jet. Indeed, as already mentioned, the primary flow of high-energy particles, accelerated by the compact source,

---

[2] The official website of the Fermi collaboration is http://fermi.gsfc.nasa.gov/.

is expected to be highly anisotropic, with the direction set by the magnetic field in the acceleration region. The cascades produce a stream of relativistic particles with velocities scattered within some angle ζ around the direction of the primary flow. From the kinematical point of view, such a stream is nothing else than a blob of plasma moving with the bulk Lorentz factor

$$\Gamma \simeq \frac{1}{\zeta} . \tag{34}$$

The angle ζ is determined by the dynamics of the cascade. An important role in this dynamics is played by the value and configuration of the magnetic field. At the late stages of the cascade development, when the density of the particles in the cascade is large, the problem should be solved self-consistently taking into account the back-reaction of the plasma in the cascade on the magnetic field. This observation makes the link between the cascade and the blob pictures not only kinematical but also dynamical: in the standard approach, the magnetic field is also determined self-consistently by the dynamics of the blob itself.

Existence of this link enables us to use in the analysis of TeV γ-ray flares within the framework of the compact source models many results from the standard approach. In particular, the transparency of the blob for the TeV radiation in the 2006 July large flare of PKS 2155−304 implies the constraint (Begelman et al. 2008) $\Gamma \gtrsim 50$ and hence, $\zeta \lesssim 1°1$.

On the other hand, there are several important differences between the cascade and a generic relativistic blob model which potentially enable us to distinguish the two models observationally. First, in the cascade setup, the relativistic blobs are formed in a compact region close to the BH. In this way, this setup naturally incorporates the observed fast variability and is not in a direct conflict with the low bulk Lorenz factors observed at the parsec-scale distances. Indeed, the bulk motion of the secondary particles in the cascade can decelerate at parsec-scale distances either because of development of intrinsic instabilities or interaction with the interstellar medium. To study this possibility, a dynamical numerical calculation of the propagation of the high-energy particle cascade through the accretion flow and the interstellar medium is needed. Secondly, the cascade transfers power from the higher energy particles to the lower energy ones: in this sense, it is a 'top-down' scenario of formation of the spectrum of emitting electrons. It would be interesting to understand if the latter property can explain the existence of the low-energy cut-offs in the spectra of electrons in the synchrotron – IC scenarios (Krawczynski 2007). Finally, as already mentioned, in the compact source model, the emission from the blob may be superimposed on to the γ-ray component originating directly in the acceleration region near the BH.

3 TIMING OF THE SUPERMASSIVE BLACK HOLE IN PKS 2155−304 WITH TeV γ-RAYS

Within the compact source model, the spectral and variability properties of the VHE signal can be interpreted in a qualitatively different way (as compared to the model of VHE emission from the parsec-scale distances). They can be used to 'probe' the physical environment in the central engine: the matter density, the radiative efficiency of the accretion flow and the magnetic field (cf. Rieger & Aharonian 2008b). Moreover, in this case the VHE observations provide a completely new tool for the study of the BH physics. Namely, the γ-ray timing data can be used to derive constraints on the parameters of the BH itself. Below we explore such a possi-

bility on a particular example of the 2006 July large flare of PKS 2155−304 (redshift $z = 0.116$) reported by Aharonian et al. 2007.

3.1 The relevant time-scales

Timing properties of emission produced in the vicinity of BH horizon can be characterized by several fundamental time-scales. First, the minimal possible variability time-scale is determined by the requirement of causal connection of the emission region and given by the light-crossing time of the BH horizon,

$$\begin{aligned} t_{\mathrm{lc}} &= 2 \left(R_{\mathrm{g}} + \sqrt{R_{\mathrm{g}}^2 - a^2} \right)/c \\ &\simeq \begin{cases} 10^2 \left(M_{\mathrm{BH}}/10^7 \, \mathrm{M_\odot} \right) \mathrm{s}, & a = R_{\mathrm{g}}, \\ 2 \times 10^2 \left(M_{\mathrm{BH}}/10^7 \, \mathrm{M_\odot} \right) \mathrm{s}, & a = 0, \end{cases} \end{aligned} \tag{35}$$

where R_{g} is defined in equation (2); the parameter a is related to the angular momentum J_{BH} of the BH as $a = J_{\mathrm{BH}}/M_{\mathrm{BH}} c^2$ and lies in the range $0 \leq a \leq R_{\mathrm{g}}$.

If the γ-ray emission is produced close to the BH, variability at the characteristic time-scale of rotation around the BH is expected on general grounds, unless the entire system (the accretion flow with an embedded particle acceleration region) is perfectly axially symmetric. The intensity of the modulation of the signal can depend on various parameters, such as the inclination angle of the observer with respect to the BH rotation axis, distance of the emission region from the horizon, etc. A perfect axial symmetry, which would wash out the modulation of the signal with the period of rotation around the BH, can be expected in a stationary, quiet state of the source. On the contrary, a bright flare is, most probably, related to the rapid change of the system parameters (e.g. inspiralling of a denser clump of matter into the BH) which should lead to a significant disturbance of the axially symmetry.

Close to the horizon of a spinning BH, the accreting matter rotates around the BH with the period (Bardeen, Press & Teukolsky 1972):

$$P(r) = 2\pi \frac{r^{3/2} \pm a R_{\mathrm{g}}^{1/2}}{c R_{\mathrm{g}}^{1/2}} , \tag{36}$$

where r is the radius of the orbit. The $+ (-)$ sign corresponds to the prograde (retrograde) orbit. It is known that stable circular orbits exist only down to certain distance r_{ms} from the BH. The period of rotation along the last prograde stable orbit at the distance r_{ms} is

$$P(r_{\mathrm{ms}}) = \begin{cases} 4\pi R_{\mathrm{g}}/c \simeq 630 \left(\dfrac{M_{\mathrm{BH}}}{10^7 \, \mathrm{M_\odot}} \right) \mathrm{s}, & a = R_{\mathrm{g}} \\ 12\sqrt{6}\pi R_{\mathrm{g}}/c \simeq 4600 \left(\dfrac{M_{\mathrm{BH}}}{10^7 \, \mathrm{M_\odot}} \right) \mathrm{s}, & a = 0. \end{cases} \tag{37}$$

The disturbance of the axial symmetry of the accretion flow is expected to result in the modulation of physical conditions in the AGN central engine with a period given by equation (37). Since the properties of the γ-ray emission from the central engine (from the base of the jet) are determined by the physical conditions in the central engine, the modulation of these conditions should result in the modulation of the γ-ray signal with the same period.

3.2 Fitting the light curve of PKS 2155−304

The VHE γ-ray light curve of the flare of PKS 2155−304, reported in Aharonian et al. 2007, consists of several pronounced subflares (see Fig. 2). At least three characteristic time-scales can be found in a straightforward way from the analysis of the light curve: the rise and decay times of the individual subflares, t_{rise}, t_{decay}, and the period of
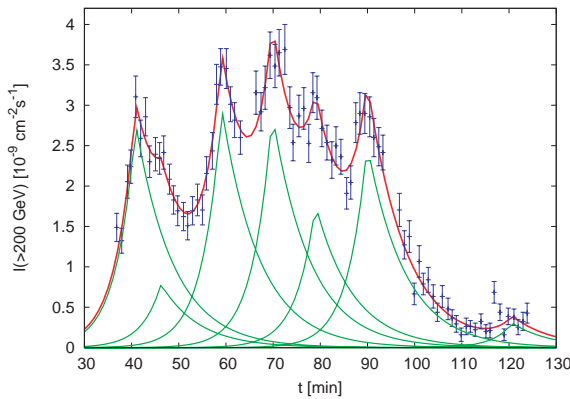
Figure 2. The light curve of PKS 2155−304 fitted with a sequence of sub-flares with identical profiles, but with different normalizations (see Table 1).

Table 1. List of parameters of the subflares.

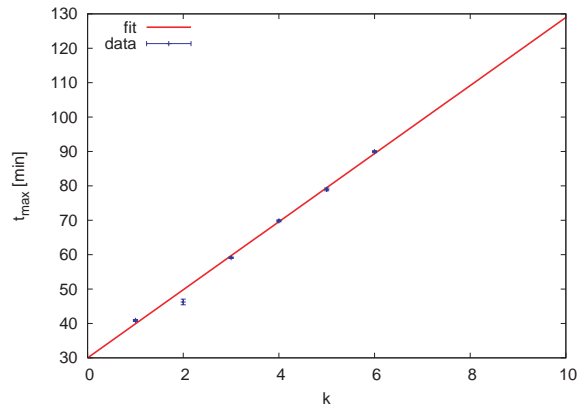| k	$t_{\mathrm{max},k}$ (min)	$N_k (10^{-9}\,\mathrm{cm}^{-2}\,\mathrm{s}^{-1})$
1	40.9 ± 0.3	2.8 ± 0.3
2	46.2 ± 0.8	0.78 ± 0.24
3	59.1 ± 0.2	3.0 ± 0.17
4	69.8 ± 0.3	2.9 ± 0.2
5	79.0 ± 0.4	1.8 ± 0.2
6	89.9 ± 0.3	2.5 ± 0.2
9	120.7 ± 1.0	0.30 ± 0.11

Figure 3. The arrival times of the subflares of the PKS 2155−304 light curve as a function of the subflare number. The data are fitted by the straight line $t_{\mathrm{max},k} = t_0 + kT$.

recurrence of the subflares, T. In order to estimate the average values of these parameters, we have fitted the VHE light curve assuming that the time profiles of the individual subflares are characterized by the same rise and decay times, and differ only in the arrival times and the amplitudes.[3] The approximation of identical t_{rise}, t_{decay} appears naturally in the context of the compact source models where these parameters are determined by the intrinsic time-scales of the central engine, such as, for example, the light-crossing time of the BH and the cascade development time. On the other hand, it is clearly a strong idealization: the complicated dynamics of the particle acceleration and the cascade development is expected to introduce a scatter in the characteristics of the individual subflares. Still, we stick to this approximation as a natural first step.

The individual subflares are modelled with the profile

$$I_k(t) = \begin{cases} N_k \exp[(t - t_{\mathrm{max},k})/t_{\mathrm{rise}}], & t < t_{\mathrm{max},k} \\ N_k \exp[-(t - t_{\mathrm{max},k})/t_{\mathrm{decay}}], & t > t_{\mathrm{max},k}, \end{cases} \quad (38)$$

where the time $t_{\mathrm{max},k}$ corresponds to the maximum intensity and N_k is the amplitude of the kth subflare. Note that we define $t_{\mathrm{rise}}(t_{\mathrm{decay}})$ as the time in which the signal increases (decreases) by a factor of e. We fit the light curve with the sum of several subflares (equation 38) and a constant signal. The result of the fit of the overall light curve with such a model is shown in Fig. 2. The rise and decay times inferred from the fit are

$$t_{\mathrm{rise}} = (2.5 \pm 0.2) \times 10^2\,\mathrm{s}, \quad (39)$$

$$t_{\mathrm{decay}} = (4.9 \pm 0.5) \times 10^2\,\mathrm{s}. \quad (40)$$

The arrival times $t_{\mathrm{max},k}$ and normalizations N_k of the subflares are summarized in the Table 1.

Initially, we fitted the light curves with a set of five subflares which correspond to the five pronounced peaks clearly visible in the data. The quality of this fit was rather low [$\chi^2 = 106$ for 70 degrees of freedom (d.o.f.)]. We have found that the addition of one more subflare (subflare number 2 in Table 1) significantly improves the quality of the fit ($\chi^2 = 86.3/68$ d.o.f.; the F-test gives a chance probability of the fit improvement at the level of 0.1 per cent). Finally, we have found that the fit can further be improved by the addition of one more subflare near the end of the overall light

curve, the last subflare in the Table 1. The quality of the fit with seven subflares is $\chi^2 = 75.8/66$ d.o.f. According to the F-test, the probability that the latter fit improvement is achieved by chance is 1.4 per cent.

The arrival times of the six bright subflares follow an approximate linear law

$$t_{\mathrm{max},k} \simeq t_0 + kT, \quad (41)$$

see Fig. 3. This is reminiscent of quasi-periodic oscillations observed in the X-ray band in the X-ray binaries (van der Klis 2000) and the infrared band in the Galactic Centre (Genzel et al. 2003). The last weak subflare also falls on the linear dependence (equation 41) if assigned the number $k = 9$. However, we do not use this subflare in the following analysis because its presence is not strongly required by the light-curve fit.

Fitting the set of arrival times $t_{\mathrm{max},k}$ of the six bright subflares (numbered by 1–6 in the Table 1) with the linear law (equation 41), one finds the recurrence period of the subflares:

$$T = (5.93 \pm 0.15) \times 10^2\,\mathrm{s}\,. \quad (42)$$

This recurrence period coincides with the characteristic variability scale $\sim$600 s mentioned by Aharonian et al. (2007).

We have tested if the apparent quasi-periodicity of the signal can appear in the data by chance. To do this, we have fixed the arrival times of the first and last of the bright subflares (subflares 1 and 6 in the Table 1). Then, we have allowed the arrival times of the four intermediate subflares to be distributed randomly between $t_{\mathrm{max},1}$ and $t_{\mathrm{max},6}$. The arrival times $t_{\mathrm{max},k}$, $k = 1, \ldots, 6$ are assigned the errors from Table 1. We have calculated the probability that fitting the arrival times of the six first subflares by the function (equation 41) would result in a $\chi^2 \leq \chi_0^2$, where $\chi_0^2 = 41$ is the χ^2 of the fit of
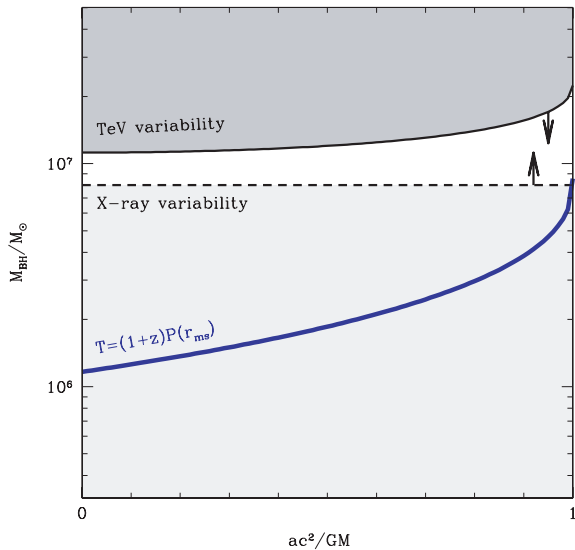
---

[3] This model is different from the model considered by Aharonian et al. (2007) where the rise and decay times were allowed to vary among individual subflares.

Figure 4. The parameters of the supermassive BH in PKS 2155−304 inferred from the VHE γ-ray light curve. The shaded region shows the range of M_{BH}, a excluded by the requirement (equation 43). Thick blue curve shows the relation between M_{BH} and a obtained by identifying the period of the subflare recurrence with the rotation period over the last stable orbit. The horizontal line shows the lower bound on the BH mass implied by the X-ray variability analysis of (Zhang et al. 2005). For $a > 0$, this bound should be taken with caution as its dependence on a has not been explored.

the real data.[4] This probability turns out to be 1.3×10^{-3}. We also tried another error assignment. Namely, all the arrival times were assigned the error $\delta t = 1.5$ min, which corresponds to the intrinsic scatter of the arrival times of the real subflares around the linear law (equation 41). In this case, the best linear fit corresponds to $\chi_1^2 = 5.43$ for 4 d.o.f. The chance probability to obtain $\chi^2 \leq 5.43$ in the simulated data sets with random arrival times of the intermediate subflares turns out to be 6×10^{-3} in this case. We have checked that our conclusions do not depend on the particular choice (equation 38) of the subflare profile by considering other possible choices of $I_k(t)$.

3.3 Constraints on the black hole parameters

The rise and decay times (equation 39), (equation 40) as well as the recurrence time (equation 42) are determined by the physics of the γ-ray emission. Within the compact source scenario described in Section 2, the minimal possible rise time is given by the light-crossing time of the BH, equation (35). Requiring

$$t_{\text{rise}} \geq (1 + z)t_{\text{lc}} \qquad (43)$$

one finds a range of parameters M_{BH}, a excluded by the observations. This range corresponds to the dark shaded region in Fig. 4.

This should be compared with the constraints obtained by the other methods. In the literature, there are two estimates of the mass of the central BH in PKS 2155−304.

The first one (Aharonian et al. 2007) is obtained from the relation between the masses of central BHs and luminosities of host galaxy bulges (Bettoni et al. 2003); it gives $M_{BH} \sim 10^9 \, M_\odot$. As it was

---

[4] Note that χ_0^2 is large. This means that the oversimplified model of strictly identical subflares with strictly periodic arrival times is actually excluded by the data. This is not surprising: as already mentioned, on physical grounds one expects deviations from this idealization.

already noted in Aharonian et al. 2007, this estimate is in conflict with the constraint $M_{BH} \leq 2 \times 10^7 \, M_\odot$ derived from the γ-ray variability properties. We point out, however, that there are several uncertainties in the estimate based on the M_{BH}–L_{bulge} relation. It is obtained by extrapolating the empirical relation observed in a local sample of normal galaxies to the case of TeV blazars. The reliability of this extrapolation was never investigated. Besides, the relation itself has a large intrinsic scatter (order-of-magnitude deviations are present). Finally, there is no consensus in the literature about the luminosity of the host galaxy in PKS 2155−304 (see Aharonian et al. 2007, and references therein).

The second estimate (Zhang et al. 2005) is based on the study of X-ray variability properties of PKS 2155−304: it uses the method of Nikolajuk, Papadakis & Czerny 2004 to relate the mass of BH to the excess variability σ_{nxs}^2 at a certain frequency scale. This method yields the bound $M_{BH} \geq 8.1 \times 10^6 \, M_\odot$ shown by a dashed horizontal line in Fig. 4. The latter estimate is compatible with the constraint derived from the TeV variability of the source. One should note, however, that the estimate of the BH mass based on the X-ray variability properties suffers from the same uncertainty as the estimate based on the M_{BH}–L_{bulge} relation: it is originally derived for a sample of nearby non-blazar AGN. Its applicability to the sample of the TeV blazars was never tested.

The tight constraint on the BH mass, derived from the TeV variability time-scale, provides a possibility of strong observational test of the compact source model. Indeed, a precise determination of the BH mass by another method would be able to falsify or confirm the compact source model.

The indication of the quasi-periodicity of the subflare arrival times suggests to associate the period T of the subflare recurrence with the (minimal possible) period of rotation around the BH:

$$T = (1 + z)P(r_{\text{ms}}). \qquad (44)$$

This gives a relation between a and M_{BH} shown by the thick blue curve in Fig. 4. If combined with the constraint on the BH mass derived from the X-ray variability analysis (Zhang et al. 2005), this relation implies that the BH is rotating almost at the maximal rate, $a \approx R_g$. However, we remind that the X-ray constraint on the BH mass should be taken with caution. In particular, to the best of our knowledge, the dependence of this phenomenological constraint on the BH spin a has not been explored.

4 CONCLUSIONS

In this paper, we have proposed that the recently observed fast variability of the VHE emission from blazars can be naturally accommodated within the framework of 'compact source' model. In this model, particles responsible for the observed VHE emission are accelerated close to the central supermassive BH, rather than at large distances downstream the AGN jet. We have analysed the problem of escape of the VHE γ-rays from the vicinity of the central engine and demonstrated that the region around the central engine is transparent for TeV γ-rays if the accretion flow in the TeV blazars is radiatively inefficient. If the luminosity of the accretion flow is as low as $L_{\text{acc}} \lesssim 10^{40}$ erg s^{-1}, the TeV γ-ray emission can come directly from the immediate neighbourhood of the central BH. Alternatively, for brighter accretion flows, the TeV γ-rays may be produced at some distance from the BH in a proton-initiated electromagnetic cascade developing in the accretion flow.

The possibility that the properties of the VHE γ-ray emission are directly linked to the properties of the central engine of the AGN, if confirmed by future observations, provides a new tool to study the

physical conditions in the direct vicinity of the supermassive BH. In particular, the VHE signal can be used to constrain the parameters of the accretion flow and the BH itself, such as its mass and spin.

We demonstrated this possibility on the example of the bright TeV flare of the blazar PKS 2155−304. Within the proposed scenario, the characteristic time-scales, found in the timing analysis of this flare, are directly related to the parameters of the supermassive BH. The minimal variability time-scale of the signal is identified with the BH light-crossing time. This sets the bound on the BH mass and its rotation moment shown in Fig. 4. We also observed that the signal exhibits quasi-periodic oscillations. Identifying the recurrence time of these oscillations with the period of rotation around the BH, we obtained a relation between the BH mass and its rotation moment.

A detailed modelling based of the framework proposed in this paper should involve calculation of particle acceleration and propagation in the vicinity of the BH through the environment created by the accretion flow. This can be done assuming particular (numerical) models of RIAF and particle acceleration. We leave this for future work.

REFERENCES

Aharonian F., Neronov A., 2005, ApJ, 619, 306
Aharonian F. et al., 2003, A&A, 403, L1
Aharonian F., Akhperjanian A. G., Bazer-Bachi A. R. et al., 2006, Sci, 314, 1424
Aharonian F. et al., 2007, ApJ, 664, L71
Albert J. et al., 2007, ApJ, 669, 862
Albert J. et al., 2008, ApJ, 685, L23
Bardeen J. M., Press W. H., Teukolsky S. A., 1972, ApJ, 178, 347
Bednarek W., Protheroe R. J., 1999, MNRAS, 302, 373
Begelman M. C., Fabian A. C., Rees M. J., 2008, MNRAS, 384, L19
Bettoni D., Falomo R., Fasano G., Govoni F., 2003, A&A, 399, 869
Blandford R. D., Levinson A., 1995, ApJ, 441, 79
Browne I. W. A., 1983, MNRAS, 204, 23P
Celotti A., Fabian A. C., Rees M. J., 1998, MNRAS, 293, 239
Genzel R., Schödel R., Ott T., Eckart A., Alexander T., Lacombe F., Rouan D., Aschenbach B., 2003, Nat, 425, 934
Ghisellini G., Madau P., 1996, MNRAS, 280, 67
Giroletti M., Giovannini G., Taylor G. B., Falomo R., 2004, ApJ, 613, 752
Giroletti M., Giovannini G., Taylor G. B., Falomo R., 2006, ApJ, 646, 801
Henri G., Saugé L., 2006, ApJ, 640, 185
Heiselberg H., 2001, Phys. Rep., 351, 161
Kardashev N. S., 1995, MNRAS, 276, 515
Krawczynski H., 2007, ApJ, 659, 1063
Levinson A., 2000, Phys. Rev. Lett., 85, 912
Lesch H., Pohl M., 1992, A&A, 254, 29
Lovelace R. V. E., 1976, Nat, 262, 649
Lu J.-F., Li S.-L., Gu W.-M., 2004, MNRAS, 352, 147
Narayan R., 2002, in Gilfanov M., Sunyaev R., Churazov E., eds, Lighthouses of the Universe: The Most Luminous Celestial Objects and Their Use for Cosmology. Springer-Verlag, Berlin, p. 405
Narayan R., Yi I., 1994, ApJ, 428, L13
Narayan R., Yi I., 1995, ApJ, 452, 710
Neronov A., Aharonian F. A., 2007, ApJ, 671, 85
Neronov A. Y., Semikoz D. V., 2002, Phys. Rev. D, 66, 123003
Neronov A., Semikoz D., 2003, New Astron. Rev., 47, 693
Neronov A., Semikoz D., Aharonian F., Kalashev O., 2002, Phys. Rev. Lett., 89, 051101
Neronov A., Tinyakov P., Tkachev I., 2005, J. Exp. Theor. Phys., 100, 656 (Zh. Eksp. Teor. Fiz. 100, 744)
Neronov A., Semikoz D., Tkachev I., 2008, Ultra-High Energy Cosmic Ray production in the Polar Cap Regions of Black Hole Magnetospheres, JETP, preprint (arXiv:0712.1737)
Nikolajuk M., Papadakis I. E., Czerny B., 2004, MNRAS, 350, L26
Pacholczyk A. G., 1970, Radio Astrophysics. W.H. Freeman and Company, San Francisco
Piner B. G., Pant N., Edwards P. G., 2008, ApJ, 678, 64
Rees M. J., Begelman M. C., Blandford R. D., Phinney E. S., 1982, Nat, 295, 17
Rieger F. M., Aharonian F. A., 2008a, A&A, 479, L5
Rieger F. M., Aharonian F. A., 2008b, preprint (arXiv:0805.4075)
Rybicki G. B., Lightman A. P., 2004, Radiative Processes in Astrophysics. Wiley-VCH, New York
van der Klis M., 2000, ARA&A, 38, 717
Zhang Y. H., Treves A., Celotti A., Qin Y. P., Bai J. M., 2005, ApJ, 629, 686

APPENDIX A: SYNCHROTRON SELF-ABSORPTION IN THE ACCRETION FLOW

The function $I(x)$ entering into the expression (14) for the synchrotron self-absorption coefficient has the form (Pacholczyk 1970),

$$I(x) = \frac{1}{x} \int_0^\infty z^2 e^{-z} F(x/z^2) dz, \tag{A1}$$

where $F(x) = x \int_x^\infty K_{5/3}(z) dz$. It is straightforward to obtain the asymptotics of $I(x)$:

$$I(x) \sim \sqrt{2/3\pi} \exp[-3(x/4)^{1/3}], \quad x \gg 1. \tag{A2}$$

The synchrotron photons are self-absorbed below a certain energy ϵ_{SA}. The latter is estimated from the condition that the optical depth for the synchrotron emission with energy ϵ_{SA} is equal to unity:

$$\alpha_{SA}(\epsilon_{SA}) R_{synch} = 1, \tag{A3}$$

where R_{synch} is the size of the synchrotron emission region. Taking $R_{synch} \approx R_g$, one obtains the following equation for the variable[5] x_{SA} corresponding to the self-absorption energy ϵ_{SA}:

$$1.89 x_{SA}^{1/3} + \ln x_{SA} = 17.37$$
$$+ \ln\left\{ \left(\frac{n}{10^{10}\,cm^{-3}}\right) \left(\frac{M_{BH}}{10^7\,M_\odot}\right) \left(\frac{B}{10^4\,G}\right)^{-1} \left(\frac{T_e}{1\,MeV}\right)^{-5} \right\}. \tag{A4}$$

When the logarithm in the second line vanishes, the solution to this equation is

$$x_{SA} = 247. \tag{A5}$$

This corresponds to the value (equation 16) of the self-absorption energy. Note that the right-hand side of the equation (A4) logarithmically depends on the parameters of the accretion flow implying that the variable x_{SA} is only mildly sensitive to these parameters. Namely, the value (equation A5) is multiplied by a factor ranging from 0.6 to 1.5 when the combination of the parameters entering the logarithm in the second line of equation (A4) varies from 0.1 to 10.

---

[5] See equation (15) for the definition of this variable.

This paper has been typeset from a TEX/LATEX file prepared by the author.